An Adaptive Framework Coping with Dynamic Target Speed for Device-Free Passive Localization

Xiuyuan Zheng, Jie Yang, *Member, IEEE*, Yingying Chen, and Hui Xiong, *Senior Member, IEEE*

Abstract—The problem of device-free passive localization aims on locating moving objects which do not carry any localization devices. The rationale of this problem is based on the fact that a moving object can result in the changes of received signal strength (RSS) of the wireless links. Existing studies on this problem usually do not consider the impact of dynamic target speed on device-free passive localization. However, the experiments show that the localization performance degrades substantially when an object is moving at dynamic speed. To meet this challenge, in this paper, we propose an adaptive device-free passive localization framework which has three components to detect target speed change and perform adaptive localization. This framework can be easily adapted for existing device-free localization methods which are based on the detection of signal strength changes. As demonstrated in the experiments, the proposed framework can lead to 50 and 30 percent improvement on median and maximum error respectively over the localization algorithms without considering dynamic moving speeds of the target.

Index Terms—Device-free localization, signal strength, wireless networks, speed change detection

1 Introduction

Device-free passive localization is an emerging technology to locate people without attaching any radio device to them in pervasive wireless environments. It has broad applications [1], [2], [3] in intrusion detection in industrial facilities for asset protection, identification of people trapped in a fire building during emergency evacuation, elder care, and battlefield protection. In these applications, we do not expect people to carry any radio devices, and thus the traditional localization techniques [4], [5], [6], which require wireless devices attached to people to emit wireless signals to assist localization process, are not applicable. With the widespread deployment of wireless devices, it is possible to capture the wireless environmental changes caused by people or intruders who move into the wireless environments. Therefore, device-free passive localization has drawn much attention recently for motion detection and target localization in pervasive wireless environments.

More than one modalities of wireless signal measurements, such as RSS [7], [8], channel impulse response in ultra wide band (UWB) [9], and polarization [10], have been utilized to facilitate device-free localization. Among all these modalities, RSS is especially attractive as the RSS readings are readily available in the existing wireless infrastructure, and thus is cost-effective. As a result, there has been increasing interests in employing RSS for device-free passive localization recently [1], [8].

Existing RSS-based device-free passive localization systems mainly rely on the changes of variance of RSS measurements from wireless links to locate the target (e.g., intruders or victims) since a large value of variance on a wireless link infers there is a target moving in the vicinity of that particular link [1], [2], [11], [12]. For instance, Wilson and Patwari deployed a RF-based sensor network around a residential house and used RSS sample variances during a time window to localize and track people inside the house [8]. These RSS-based systems do not consider the impact of dynamic target speed on the performance of passive localization, and thus the time window of calculating variance is selected as a fixed value. In practice, however, the target to be located will most likely move at dynamic speed. For example, people trapped inside a building during emergency evacuation tend to run around to escape with various speeds. Also, the intruders of an industrial facility may move at different speeds when approaching different sections of the facility. Therefore, the assumption that the target is moving at constant speed is not proper and may result in huge impact on the localization performances.

Indeed, in this paper, we first conduct a set of experiments to empirically study the impact of different moving speeds on the localization performances. We find significant performance degradation on existing RSS-based device-free localization algorithms because of ignoring the speed change of the moving target. To cope with this challenge, we propose an adaptive speed change detection framework to improve localization performances over existing device-free localization systems leveraging the changes of signal strength. Our framework consists of three components: speed change detection, determining the size of time

- *X. Zheng and Y. Chen are with the Department of Electrical and Computer Engineering, Stevens Institute of Technology, Hoboken, NJ 07030. E-mail: {xzheng1, yingying.chen}@stevens.edu.*
- *J. Yang is with the Department of Computer Science, Florida State University, Tallahassee, FL 32306. E-mail: jie.yang@cs.fsu.edu.*
- *H. Xiong is with the Department of Management Science and Information Systems, Rutgers—The State University of New Jersey, 110 Washington St., Newark, NJ 07102. E-mail: hxiong@rutgers.edu.*

Manuscript received 21 Jan. 2014; revised 11 June 2014; accepted 5 Aug. 2014. Date of publication 12 Aug. 2014; date of current version 1 May 2015. For information on obtaining reprints of this article, please send e-mail to: reprints@ieee.org, and reference the Digital Object Identifier below. Digital Object Identifier no. 10.1109/TMC.2014.2347303

window, and passive localization. To capture the target speed changes, we design three speed change detection schemes, including average variance ratio (Detection-AVR), variance distribution similarity (Detection-VDS), and likelihood ratio test (Detection-LRT), by utilizing statistical techniques to capture moving speed changes based on information obtained by RSS measurements over wireless links. Based on the speed change detection results, we adaptively adjust the time-window size, which is used to calculate variance, to facilitate accurate passive localization. Finally, we propose a new algorithm, called RIG, which is inspired by Algebraic Reconstruction in computational tomography [13]. RIG does not require tedious environmental parameter tuning when performing passive localization. We summarize our main contributions as follows:

- We illustrate that the performances of existing RSS-based device-free localization systems degrade when the target is moving at dynamic speed. Indeed, there is a need of developing adaptive device-free localization techniques to handle the objects with dynamic speeds.
- We propose an adaptive device-free localization framework. Also, we design three different speed change detection schemes based on statistical learning techniques. The proposed framework is a general framework, which is widely suitable for device-free localization systems using signal strength.
- We develop a new passive localization algorithm, named RIG, which is based on Algebraic Reconstruction. RIG uses triangle-based geometric pivot points to reduce the position estimation error in addition to using computational tomography.
- Experiments in a real-world environment validate the effectiveness of our proposed framework in coping with dynamic target speed. The results show that our speed change detection framework can obtain 50 percent improvement on median error and 30 percent improvement on maximum error compared with existing device-free localization systems.

Overview. The rest of the paper is organized as follows. We summarize related studies in Section 2. In Section 3, we introduce the framework overview and experimental methods used in the paper. Section 4 shows the analysis of the impact of dynamic target speed on the performances of device-free localization. Section 5 gives three speed change detection schemes based on statistical learning. In Section 6, we show how to adjust time-window sizes adaptively to facilitate passive localization. Section 7 presents the new device-free localization algorithm and shows the performance evaluation. Finally, Section 8 concludes the work.

2 Related Work

There is great potential for device-free passive localization in a variety of areas. Methods in prior work employ different sensing modalities to achieve motion detection and device-free passive localization [1], [9], [10]. For instance, Pratt et al. proposes to use differential polarization of EM wave at the receiver to detect object movement [10]. The impulse response from multi-path measurements of UWB is leveraged to track the object [9]. The Cramer-Rao lower bound (CRLB) is derived in different scenarios to analyze the estimation accuracy of the proposed scheme. Furthermore, a short-range radar system is developed by utilizing UWB communication [14], which is operating around 10 GHz and can penetrate walls. Youssef et al. [1] demonstrate using RSS to perform device-free localization, which is among the first works in this area.

It is popular to perform device-free localization through RSS measurements, since RSS is widely available from commodity wireless devices. Generally, there are two types of schemes: fingerprint-based and model-based. Fingerprint-based methods conduct training first and estimate target's locations by comparing the measurements during the online phase with the training measurements [3], [7], [15], [16], [17], [18], [19], [20]. The maximum likelihood estimator is proposed to perform device-free passive detection in a real environment [18]. In large-scale environments, a fingerprint method based on probabilistic techniques is introduced to locate multiple objects at the coarse-grained zones level [19], [20]. The characteristics of signal dynamics for wireless links when one or multiple targets are moving across have been studied [7], [17], where they construct a signal dynamic model to obtain the changing behaviors of RSS variance caused by the moving target. Furthermore, probabilistic classification methods are proposed in [3] to mitigate the adverse impact of cluttered indoor environments. Viani et al. [15], [16], [21], [22], [23] propose a class of approaches to recast the device-free passive localization as an electromagnetic inverse problem, and support vector machine (SVM) classifier is applied to solve the problem. For instance, learning by example (LBE) approach based on a multi-class SVM classifier is utilized to measure the real-time RSS data of wireless links [16], [22], [23]. Differential RSS measurements are utilized to filter out the environment contribution and to estimate the position of the moving target [21]. The training process aims to define the unknown inverse mapping from the measured RSS data to the target position. Furthermore, a wireless architecture [24] for estimating the presence, movements and behaviors of inhabitants as well as the insights of state-of-the-art solutions are provided.

Model based algorithms [8], [11], [25] utilize RSS variance-based radio tomographic imaging (RTI) to reduce noise effect and infer people's location from its returned image. Wilson and Patwari. introduce tomographic imaging to device-free localization [11], and we compare our proposed algorithm to this model in this paper. Furthermore, a statistical model is proposed to relate RSS variance to physical location of the moving target by using a motion image [8]. Compressive sensing based Tomography combines RF tomography and compressed sensing techniques to accurately infer environment characteristics [25]. The subspace decomposition method is further applied to RTI [26], which improves the robustness of position estimates. Particle filter based tracking approach is proposed [27], [28] by incorporating an on-line expectation maximization (EM) procedure to improve RTI with more efficiency and higher accuracy. Our proposed framework can be extended to work with

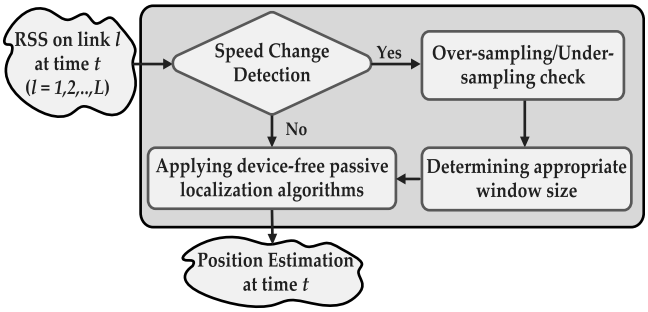

Fig. 1. Adaptive speed change detection framework overview.

these studies to improve the tracking accuracy when the target moves at dynamic speeds. Moreover, an accurate fade level based model is proposed [29] to quantify temporal fading on static links, and the location of moving target is further estimated via particle filter. The detection and tracking [30], [31] of human motion are further proposed to adapt to the changes caused by the moving object to the wireless environment. The particle filter is utilized to track the location of a moving object [31], whereas the location estimation is updated by assigning linear weights to the streaming data [30]. None of the aforementioned work has considered the impact of dynamic target speed to the performance of passive localization, which could be the case in many real-world scenarios. In this work, we aim to achieve high accuracy in device-free passive localization even when target is traveling at various speeds.

3 Framework Overview and Experimental Methodology

In this section, we first provide an overview of our proposed adaptive speed change detection framework. We then describe our experimental methodology used across the paper.

3.1 Framework Overview

Existing RSS-based device-free localization systems assume the target is moving under a constant speed. Thus, the localization system parameters are fixed during the localization process, making the current algorithms suffer from large performance degradation when target is moving with dynamic speeds. Our focus in this paper is to achieve high accuracy of device-free passive localization under dynamically changing speed of the target. To cope with dynamic moving speeds, there are two challenges: how to capture the speed changes, and how to adjust the localization system parameter adaptively based on the captured changes in speed? In our work, we propose an adaptive speed change detection framework to address these challenges as well as incorporate existing localization techniques for passive localization.

Our framework consists of three components as shown in Fig. 1: speed change detection, determining the size of time window, and passive localization. To capture target speed changes, we design three speed change detection schemes, including Detection-AVR, Detection-VDS, and Detection-LRT based on statistical learning from the information obtained from RSS measurements over wireless

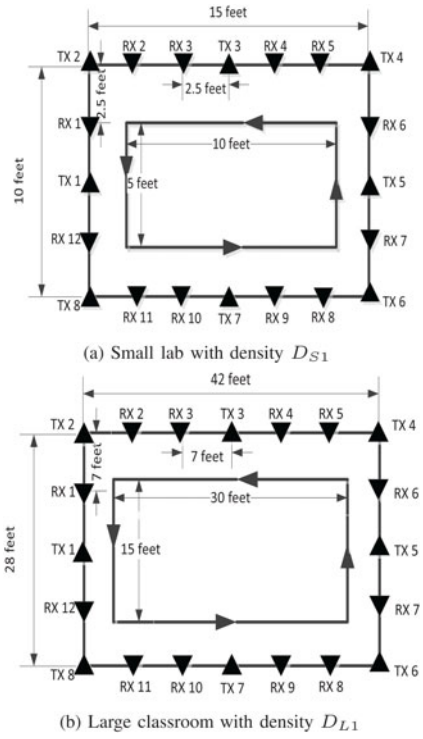

Fig. 2. Illustration of experimental deployment.

links. After the speed change is captured, we propose a time-window size determination scheme to adaptively update the localization system parameter, particularly the window size for RSS variance calculation. Additionally, we propose a new localization algorithm inspired by Algebraic Reconstruction in computational tomography, which does not require tedious environmental parameter tuning when performing passive localization. We note that our framework is generic which can incorporate any existing localization algorithms using signal strength, for example, the popular RTI method [11]. If no target speed change is detected, the localization algorithms will be applied directly with a fixed window size derived from empirical study.

3.2 Experimental Methodology

3.2.1 Experimental Setup

We conduct experiments using active RFID transmitters and receivers [32] in typical indoor multi-path environment. Each RFID tag has one antenna. The RFID system is synchronized by using the techniques provided in [33]. And each RFID tag is a transceiver, which is powered by a button battery. It can be programmed either as a transmitter or a receiver. Each RFID transmitter periodically broadcasts beacon massages with its identifier at the frequency of 900 MHz, with packet rate of four packets per second. After the receivers receive the beacon message, they extract the information of identifier together with corresponding RSS and then store it to a Linux machine that all the receivers connected to. The Linux machine, as a server, is equipped with a 2 GHz CPU, a 1 GB RAM and a 120 GB disk. Our framework is general to wireless devices of other frequency levels such as 2.4 GHz. We will provide the performance evaluation of the system using other frequency levels in our future work.

TABLE 1
Link Density in the Small Lab and Large Classroom with the Number of Transmitters and Receivers

Small lab				Large classroom			
Density	TX	RX	links/m^2	Density	TX	RX	links/m^2
D_{S1}	8	12	6.89	D_{L1}	8	12	0.88
D_{S2}	8	6	3.44	D_{L2}	8	6	0.44
D_{S3}	4	6	1.72	D_{L3}	4	6	0.22
D_{S4}	4	3	0.86	D_{L4}	4	3	0.11

3.2.2 Experimental Scenarios

We experiment with two different indoor environments: a small lab and a large classroom. The small lab with $15\,\text{ft} \times 10\,\text{ft}$ size is located on the first floor of Burchard building at Stevens Institute of Technology, as shown in Fig. 2a, whereas the large classroom with $45\,\text{ft} \times 35\,\text{ft}$ size is located on the first floor of Babbio center of Stevens Institute of Technology, as shown in Fig. 2b. The small lab is a microprocessor lab surrounded by chairs and shelves with electronic instruments on it, while the large classroom is equipped with tables and chairs inside it for lectures. The active RFID tags (denoted as TX) and readers (denoted as RX) are deployed as a rectangle along the walls inside the rooms at the height of 3 ft 2 in. The target walks along a rectangular trace of $10\,\text{ft} \times 5\,\text{ft}$ in the small lab and $30\,\text{ft} \times 15\,\text{ft}$ in the large classroom, depicted in Fig. 2. We experiment with four different speeds: *Speed 1* ($\frac{5}{8}$ ft/s), *Speed 2* ($\frac{15}{8}$ ft/s), *Speed 3* ($\frac{5}{2}$ ft/s), and *Speed 4* ($\frac{15}{4}$ ft/s). During the experiments, we change the speed using different patterns: increasing (speed $1 \rightarrow 2 \rightarrow 3 \rightarrow 4$), decreasing (speed $4 \rightarrow 3 \rightarrow 2 \rightarrow 1$), and mixture ($1 \rightarrow 4 \rightarrow 2 \rightarrow 3$).

Furthermore, we conduct experiments under different wireless link densities. The link density is defined as the number of transmitter-receiver links over unit area as shown in Table 1. The most dense link density in the small lab (D_{S1}) is similar to the link density setup in [11], and the other link densities of the small lab (D_{S2} to D_{S4}) are more sparse than the existing works. All the link densities in the large classroom (D_{L1} to D_{L4}) are more sparse than the existing work. We note that D_{S4} is equivalent to D_{L1}. To vary the link density, we reduce the transmitter and receiver in a uniform way. For example, in the small lab of density D_{S2}, based on Fig. 2a, we remove RX 1, 3, 5, 7, 9 and 11. To obtain density D_{S3}, we further remove TX 1, 3, 5 and 7. To obtain density D_{S4}, we further remove RX 2, 6 and 10. We do the similar removal for the large classroom to obtain density D_{L2} to D_{L4}.

4 Impact of Dynamic Target Speed on Device-Free Passive Localization

To understand the impact of dynamic target speed on device-free passive localization, we experiment with different walking speeds in indoors. Specifically, we define four typical speed categories [34]: very slow speed (0-1 ft/s referred as *speed 1*) (e.g., an intruder breaks into an office with caution or people is hiding behind furniture in a fire building); slow speed (1-2 ft/s referred as *speed 2*) (e.g., walking carefully); normal speed (2-3 ft/s referred as *speed 3*) (walking normally); and fast speed (3-4 ft/s referred as *speed 4*) (e.g., walking in a hurry). Existing device-free passive localization systems using signal strength mainly capture the changes of variance of RSS measurements to determine whether a target is in the area of interest [1], [2], [11], [12]. Thus, the variance of RSS measurements becomes an important metric exploited in device-free localization systems. In this paper, we use the following definition of RSS variance as our basis.

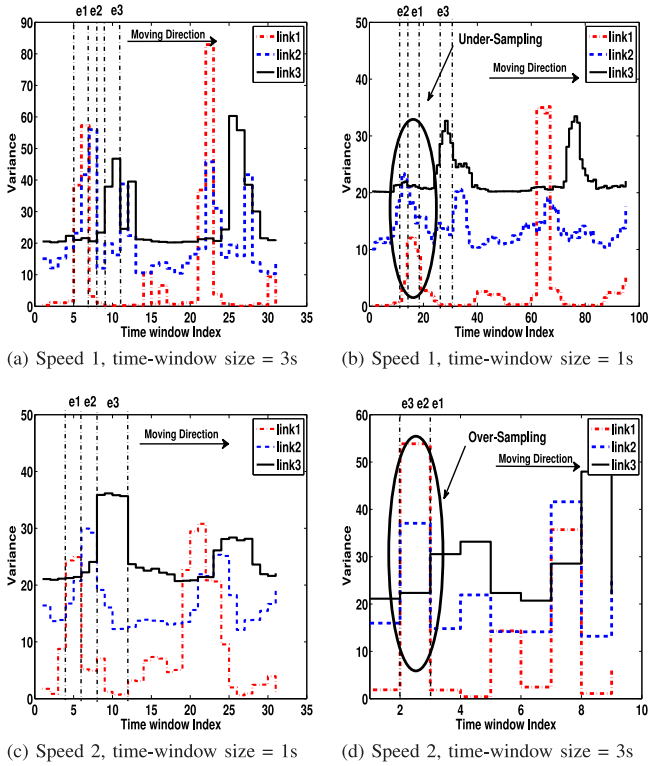

(a) Speed 1, time-window size = 3s (b) Speed 1, time-window size = 1s

(c) Speed 2, time-window size = 1s (d) Speed 2, time-window size = 3s

Fig. 3. Variance of signal strength in time series calculated with different time window under two different speeds, *Speed 1* and *Speed 2*.

We define $r_{l,W}(i)$ as the ith sample of RSS on link l in time window W, which is used to calculate variance for localization algorithms. The variance of the time window W from link l can be calculated as

$$\hat{\sigma}^2_{l,W} = \frac{1}{N-1}\sum_{i=0}^{N-1}(\overline{r}_{l,W} - r_{l,W}(i))^2, \quad (1)$$

where N is the number of RSS samples within the time window W, and $\overline{r}_{l,W} = \frac{1}{N}\sum_{i=0}^{N-1} r_{l,W}(i)$ is the sample mean of received signal strength within W. It is obvious that time window of W plays a critical role when calculating RSS variance. And a larger RSS variance value of a wireless link indicates the target is close to that particular link. Note that the number of samples N is related to the sampling rate and time window W. In our work, the sampling rate is fixed, and set to four packets per second. Thus, we only study the time window W in the following paper.

Analysis of variance calculation under different target speeds. To analyze the impact of different target speeds on the localization performance, we conduct experiments using 20 RFID tags in a $15\,\text{ft} \times 10\,\text{ft}$ student lab with link density D_{S1} as described in Fig. 2a. Fig. 3 presents the variance

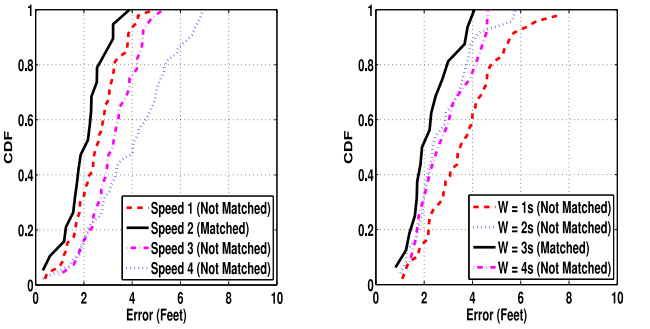

(a) Different speed, the same time window (b) Speed 1, multiple time window

Fig. 4. Device-free localization using Radio Tomographic Imaging method: (a) using the same time window $W = 1\,\mathrm{s}$ for RSS variance calculation under four different speeds; and (b) using different time window for RSS variance calculation under *Speed 1*.

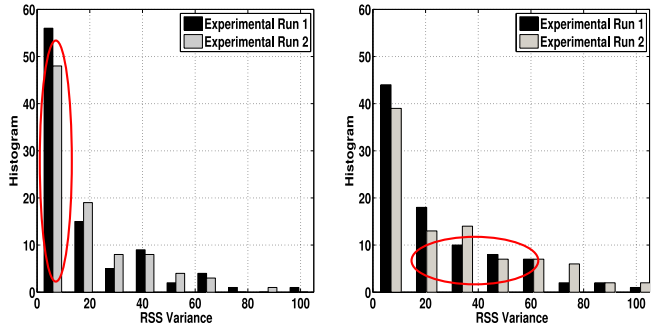

(a) Speed 1 (b) Speed 2

Fig. 5. Histogram of RSS variance by randomly choosing two experimental runs for (a) *speed 1* and (b) *speed 2* respectively with time interval $\Delta T = 2\,\mathrm{s}$.

obtained from three adjacent wireless links by using two different time window when a target is walking across these three adjacent links sequentially in the order of link $1 \rightarrow$ link $2 \rightarrow$ link 3 under *Speed 1* and *Speed 2* respectively. When the target crosses the ith link, a moving event of 'e_i' ($i = 1, 2, 3$) is derived if the change of RSS variance is above a threshold.

Fig. 3a shows the correct order of moving events (i.e., $e1 \rightarrow e2 \rightarrow e3$) derived from the calculated variance when the time window is set to $3\,\mathrm{s}$ under *Speed 1*. However, when the time window is set to $1\,\mathrm{s}$, the derived target moving order becomes $e2 \rightarrow e1 \rightarrow e3$ as depicted in Fig. 3b, which is inconsistent with the groundtruth. Turning to examine *Speed 2* (a faster speed), Fig. 3c presents the correct order of moving events (i.e., $e1 \rightarrow e2 \rightarrow e3$) obtained from the calculated variance when the time window is set to $1\,\mathrm{s}$, whereas the derived target moving order becomes mixed events $(e1, e2, e3)$ when the time window is $3\,\mathrm{s}$ as shown in Fig. 3d, which is the appropriate time window to capture the correct order of moving events under the slower speed (*Speed 1*). We thus define the scenario in Fig. 3b as *under-sampling*, since the time window $1s$ is too small to capture the correct target moving events for *speed 1*; and the scenario in Fig. 3d as *over-sampling* as the time window $3\,\mathrm{s}$ is too large for *speed 2*. This important observation indicates that appropriate time window needs to be chosen to accurately calculate RSS variance and consequently capture the target moving pattern.

Impact of speed change on device-free localization performance. We next study the impact of different speeds on device-free localization performance by using the well known RSS-based device-free localization technique, RTI method [11]. Fig. 4a shows the cumulative distribution function of the localization error when the time window W is set to $1\,\mathrm{s}$ when the target moves in four different speeds. We find that the time window $1s$ produces the best performance under *Speed 2*. Whereas the localization process introduces large localization errors under other speeds with performance degradation of 100 percent on median error and 75 percent on maximum error under *Speed 4*, the same localization algorithm RTI is applied. Similarly, when the target moves in *Speed 1*, we find that the localization results achieve smallest errors when the time window is set to $W = 3\,\mathrm{s}$, which is inline with our observation of RSS variance changes in Fig. 3a. For example, when comparing the performance under the time window of $3\,\mathrm{s}$ to that of $1\,\mathrm{s}$, we observe the median error is 80 percent better and the maximum error is about 100 percent better. The localization performance clearly shows that choosing the appropriate time-window to adaptively capture the dynamic target moving pattern is critical in resulting in accurate location estimate of the target.

5 Speed Change Detection

In this section, we present our speed change detection schemes including Detection-AVR, Detection-VDS, and Detection-LRT scheme. We further evaluate the performance of these proposed detection schemes using real data collected in a variety of experimental scenarios.

5.1 Speed Change Detection Scheme

Although the radio signal is affected by reflection, refraction, diffraction, and scattering, the RSS of the wireless links should be relatively stable if there is no movement or changes in wireless environment. However, the wireless environment will get affected and result in the changes in the RSS readings if there is people moving around. The variance of the RSS readings is thus widely used as a powerful indicator for motion detection and target localization. Furthermore, the statistical characteristics of variance of the wireless links should be different under different target speeds. In particular, the target with faster speed usually cuts more wireless links than that of slower one does, given a fixed time interval. Therefore, the number of links with significant variance changes under the faster speed should be more than that of the slower one.

Therefore, to detect the speed change, we compare the RSS variance in two adjacent observed time intervals: the current time interval ΔT and the previous time interval $\Delta T'$. These two time intervals are non-overlapping with the same size. We randomly choose two experimental runs each for two speeds (*Speed 1* and *Speed 2*) when the target moves across wireless links. The received signal variance distribution is depicted in Fig. 5. We observe that the distribution of the variance is different for different speeds. Furthermore, the same speed (i.e., the experimental runs 1 and 2 under Speed 1) exhibits similar variance distributions over the wireless links. Specifically, faster speeds (e.g., *Speed 2*)

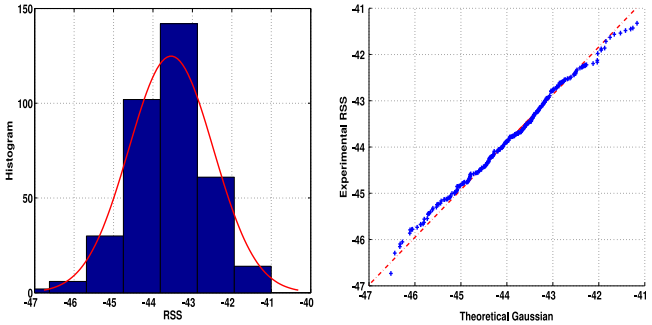

(a) With a moving target (b) Quantile-Quantile plot

Fig. 6. (a) Histogram for typical experimental RSS measurements from an arbitrary link with a moving target. The smooth curve in red is a fit of gaussian distribution. (b) Quantile-Quantile plot, where the *x*-axis represents the theoretical Gaussian quantile, and the *y*-axis represents the measured quantile.

produce more large values of RSS variance (e.g., over 10) indicating that more wireless links are affected due to significant variance changes under the faster speed. Thus, the larger the difference of the variance distribution in these two adjacent windows is, the higher probability that the target changes its speed. This motivates us to capture the statistical changes of the observed variance as a basis to design our speed change detection schemes. We note that existing works propose to detect and estimate the speed of vehicles based on statistical and curve fitting approaches [35] and differentiate between human and vehicles based on the mean and variance of received signal strength [36]. It is different from our work in that they do not perform localization, and the speed estimation approach is designed for vehicles' speed. We focus on targets in indoors by utilizing statistical methods to detect target speed change, and further adaptively adjust the time-window size to facilitate accurate passive localization. The proposed framework works with individual moving targets or multiple targets moving together. We will study the scenario of multiple targets moving separately in our future work.

5.1.1 Average Variance Ratio (Detection-AVR)

We define AVR as,

$$AVR = \frac{1}{L}\sum_{l=1}^{L}\frac{\sigma^2_{l,\Delta T}}{\sigma^2_{l,\Delta T'}} (AVR > 0), \tag{2}$$

where L is total number of links, $\sigma^2_{l,\Delta T}$ is the variance of link l for ΔT, and $\sigma^2_{l,\Delta T'}$ is the variance of link l for $\Delta T'$. When the average variance ratio AVR falls below an empirical threshold τ_1 ($0 < \tau_1 < 1$) or exceeds an empirical threshold τ_2 ($\tau_2 > 1$), we declare a speed change detected; otherwise, we declare it as no speed change. Detection-AVR is a simple scheme with lightweight computational cost that only captures coarse-grained information of variance distribution for speed change detection. We next describe Detection-VDS scheme, which can capture the distribution difference of the variance in current and previous time intervals. Note that the average variance ratio technique can be also used to detect the presence of a target in the area of interest [19].

5.1.2 Variance Distribution Similarity (Detection-VDS)

To further measure the variance distribution similarity for speed change detection, we utilize Kullack-Leibler (KL) divergence metric [37], which measures the difference between two probability distributions, in Detection-VDS scheme. When two speeds are similar, the links that are affected by the moving target at the current time interval and previous time interval should be similar, and so are the signal variance distributions under the two speeds. Thus, the KL-divergence value should be small under similar speeds. However, when two speeds are significantly different, the links that are affected by the moving target at the current time interval and previous time interval should be different. And the variance distributions under the two speeds are different enough to result in two different signal variance distributions under the two speeds. This can be observed by a large KL-divergence value.

Given the variance distributions over all links P and Q at the current time interval ΔT and previous time interval $\Delta T'$ respectively, the KL-divergence metric is defined as,

$$D_{KL}(P||Q) = \sum_{l} P(x)\ln\frac{P(x)}{Q(x)}. \tag{3}$$

We declare a speed change when $D_{KL}(P||Q)$ exceeds a threshold ε ($\varepsilon < 1$); otherwise, we declare no speed change. If the variance distribution P or Q contains a value equal to 0, we replace it with a small value ζ in order to avoid the infinite KL-divergence value, and we choose $\zeta = 0.001$ in our work. Different from Detection AVR, Detection-VDS tries to utilize a statistical method to capture the differences between two speeds by studying the fine-grained information from the probability distribution of signal variance under the two speeds.

5.1.3 Likelihood Ratio Test (Detection-LRT)

While the above two methods are straightforward, they do not model the underlying distribution of variance under different speeds. We further propose a Detection-LRT method that uses likelihood ratio test for speed change detection based on variance distribution modeling.

Gaussian approximation. We assume that the RSS measurements are Gaussian distributed. We first present experimental data to support this assumption, and then provide further derivations of our scheme. Fig. 6 shows representative histogram for those links with moving target. The corresponding Quantile-Quantile plot is depicted in Fig. 6b. Empirically, we observe that most of the links fit the Gaussian distribution well enough to produce an acceptable fit. We perform the normality test via the Jarque-Bera test and Kolmogorov-Smirnov test. Over 90 percent of the links accept the null hypothesis as a normal distribution at the 2 percent significance level.

Modeling. The RSS of the wireless links can be represented as,

$$\mathbf{r}(i) = \mathbf{s}(i) + \mathbf{n}(i), i = 0, \ldots, N-1, \tag{4}$$

where $\mathbf{r}(i) = [r_1(i) \cdots r_l(i) \cdots r_L(i)]^T$ denotes the ith sample of the received signal strength for the $L \times 1$ wireless links,

$\mathbf{s}(\mathbf{i})$ is defined as the RSS measurements when no human motion occurs, $\mathbf{n}(\mathbf{i})$ represents RSS changes due to target motion and is assumed Guassian, i.e., $\mathbf{n}(i) \sim N(0, \mathbf{\Sigma}_n)$, $\mathbf{\Sigma}_n = diag\{\boldsymbol{\sigma}_{nl}^2\}$ with $l = 1 \cdots L$ is the covariance matrix. The change of RSS readings from different wireless links are assumed independent, thus the covariance matrix $\mathbf{\Sigma}_n$ is symmetric and diagonal.

To detect the speed changes, we conduct the statistical hypothesis testing where the null hypothesis is there is no speed change H_0 and the alternative hypothesis is there exists speed changes H_1:

$$H_0 : \mathbf{r}(i) = \mathbf{s}(i) + \mathbf{n}(i)_{sp0}, i = 0, \ldots, N-1, \tag{5}$$

$$H_1 : \mathbf{r}(i) = \mathbf{s}(i) + \mathbf{n}(i)_{sp1}, i = 0, \ldots, N-1, \tag{6}$$

where $\mathbf{n}_{sp0} \sim N(0, \mathbf{\Sigma}_{sp0})$ and $\mathbf{n}_{sp1} \sim N(0, \mathbf{\Sigma}_{sp1})$. We note that $\mathbf{s}(\mathbf{i})$ can be measured when there is no target motion, thus, the mean of signal $\mathbf{r}(i)$ is known for hypothesis testing and is denoted as $\mu = (\mu_1 \cdots \mu_L)^T$. $\mathbf{\Sigma}_{sp0}$ and $\mathbf{\Sigma}_{sp1}$ are unknown parameters, which are estimated later. The RSS measurements are assumed to be Gaussian distributed in the hypothesis testing.

Performing detection. Given the RSS measurements under two hypotheses, we have conditional density functions as

$$\begin{aligned} f(\mathbf{R} \mid H_1) = & \prod_{i=0}^{N-1} \frac{1}{\sqrt{(2\pi)^L |\mathbf{\Sigma}_{sp1}|}} \\ & \times exp\left(-\frac{1}{2}(\mathbf{r}(i)-\mu)^T (\mathbf{\Sigma}_{sp1})^{-1} (\mathbf{r}(i)-\mu)\right), \end{aligned} \tag{7}$$

$$\begin{aligned} f(\mathbf{R} \mid H_0) = & \prod_{i=0}^{N-1} \frac{1}{\sqrt{(2\pi)^L |\mathbf{\Sigma}_{sp0}|}} \\ & \times exp\left(-\frac{1}{2}(\mathbf{r}(i)-\mu)^T (\mathbf{\Sigma}_{sp0})^{-1} (\mathbf{r}(i)-\mu)\right), \end{aligned} \tag{8}$$

where $\mathbf{R} = [\mathbf{r}(0) \cdots \mathbf{r}(N-1)]$.

The log-likelihood function of hypothesis testing is,

$$\begin{aligned} \ln(L(\mathbf{R})) = \sum_{i=1}^{N} \Big\{ & \frac{1}{2}\mathbf{r}(i)^T [(\mathbf{\Sigma}_{sp0})^{-1} - (\mathbf{\Sigma}_{sp1})^{-1}]\mathbf{r}(i) \\ & + \mu^T [(\mathbf{\Sigma}_{sp1})^{-1} - (\mathbf{\Sigma}_{sp0})^{-1}]\mathbf{r}(i) + \mathbf{C} \Big\}, \end{aligned} \tag{9}$$

where $\mathbf{C} = \frac{1}{2}\ln\frac{|\mathbf{\Sigma}_{sp0}|}{|\mathbf{\Sigma}_{sp1}|} + \mu^T[(\mathbf{\Sigma}_{sp0})^{-1} - (\mathbf{\Sigma}_{sp1})^{-1}]\mu$. We define $\tilde{\mathbf{y}}(i) = [(\mathbf{\Sigma}_{sp0})^{-1} - (\mathbf{\Sigma}_{sp1})^{-1}]^{\frac{1}{2}}\mathbf{r}(i)$, and $\tilde{\mu} = [(\mathbf{\Sigma}_{sp0})^{-1} - (\mathbf{\Sigma}_{sp1})^{-1}]^{\frac{1}{2}}\mu$. Then, Equation (9) can be reformed as,

$$\begin{aligned} \ln(L(\mathbf{R})) &= \frac{1}{2}\sum_{i=1}^{N} |\tilde{\mathbf{y}}(i) - \tilde{\mu}|^2 - N\tilde{\mu}^T\tilde{\mu} + N\mathbf{C} \\ &= \frac{1}{2}\sum_{i=1}^{N} |\tilde{\mathbf{y}}(i) - \tilde{\mu}|^2 + \frac{N}{2}\ln\frac{|\mathbf{\Sigma}_{sp0}|}{|\mathbf{\Sigma}_{sp1}|}. \end{aligned} \tag{10}$$

We accept H_1, if $\ln(L(\mathbf{R})) > \gamma$. Then, the test statistic can be written as,

$$\begin{aligned} T(\mathbf{R}) &= \sum_{i=1}^{N} |\tilde{\mathbf{y}}(i) - \tilde{\mu}|^2 = \sum_{i=1}^{N} |(\mathbf{\Sigma}_{sp0})^{-1} - (\mathbf{\Sigma}_{sp1})^{-1}| \cdot |\mathbf{r}(i) - \mu|^2 \\ &> 2\gamma - N\ln\frac{|\mathbf{\Sigma}_{sp0}|}{|\mathbf{\Sigma}_{sp1}|} = \gamma'. \end{aligned} \tag{11}$$

Therefore, we have

$$T'(\mathbf{R}) = \sum_{i=1}^{N} |\mathbf{r}(i) - \mu|^2 > \frac{2\gamma - N\ln\frac{|\mathbf{\Sigma}_{sp0}|}{|\mathbf{\Sigma}_{sp1}|}}{|(\mathbf{\Sigma}_{sp0})^{-1} - (\mathbf{\Sigma}_{sp1})^{-1}|} = \gamma'. \tag{12}$$

Since $\mathbf{r}(i)$ and μ are both $L \times 1$ vectors, the test statistic $T'(\mathbf{R})$ can be written as,

$$\begin{aligned} T'(\mathbf{R}) &= \sum_{i=1}^{N}\sum_{l=1}^{L}(r_l(i) - \mu_l)^2 = \sum_{i=1}^{N}\sigma_l^2 \sum_{l=1}^{L}\frac{(r_l(i)-\mu_l)^2}{\sigma_l^2} \\ &= \sum_{l=1}^{L}\left\{\sigma_l^2 \sum_{i=1}^{N}\frac{(r_l(i)-\mu_l)^2}{\sigma_l^2}\right\} = \sum_{l=1}^{L}\sigma_l^2 T_l'(\mathbf{R}) > \gamma', \end{aligned} \tag{13}$$

where $T_l'(\mathbf{R}) = \sum_{i=1}^{N}\frac{(r_l(i)-\mu_l)^2}{\sigma_l^2} \sim \chi^2(N)$, $\gamma' = \frac{2\gamma - N\ln\frac{|\mathbf{\Sigma}_{sp0}|}{|\mathbf{\Sigma}_{sp1}|}}{|(\mathbf{\Sigma}_{sp0})^{-1} - (\mathbf{\Sigma}_{sp1})^{-1}|}$, γ' can be obtained by satisfying a certain false positive rate. The test statistic $T'(\mathbf{R})$ is the weighted sum of central chi square distribution. In the literature, efficient method of the exact representations and approximation of this distribution have been well investigated. We refer the study in literature [38] for the distribution of the test statistics.

In Equation (12), $\hat{\Sigma}_{sp1}$ and $\hat{\Sigma}_{sp0}$ can be found by maximum-likelihood estimation (MLE) [39] of $f(\mathbf{R} \mid H_1)$ and $f(\mathbf{R} \mid H_0)$.

We have the estimated covariance matrix for one speed at current time interval ΔT,

$$\hat{\Sigma}_{\Delta T} = \frac{1}{N}\sum_{i=0}^{N-1}(\mathbf{r}(i) - \bar{\mathbf{r}}(i))(\mathbf{r}(i) - \bar{\mathbf{r}}(i))^T, \tag{14}$$

where $\bar{\mathbf{r}}$ is the sample mean of the ith sample for ΔT. Then, we take its diagonal as $\hat{\Sigma}_{sp1} = diag\{\hat{\Sigma}_{\Delta T}\}$. Similarly, for the previous time interval $\Delta T'$, $\hat{\Sigma}_{sp0} = diag\{\hat{\Sigma}_{\Delta T'}\}$.

5.2 Detection Performance

Metrics. To evaluate the performance of the proposed detection schemes, following metrics have been used. For each experimental scenario (small lab or large classroom) with a certain link density, we utilize over 600 testing cases to evaluate the performance of our detection schemes.

- *True positive (TP)* is defined as declaring speed changes when there exists a speed change.
- *False positive (FP)* is defined as declaring speed changes when there is no speed change.
- *False negative (FN)* is defined as declaring no speed change when there exists a speed change.
- *Detection accuracy (Acc)* is defined as the percentage of the trials that are correctly detected as speed change or no speed change.

TABLE 2
Detection Performance of Our Speed Change Detection Schemes in the Small lab with Density D_{S1} and Large Classroom with Density D_{L1} and Time Interval $\Delta T = 1, 3, 5$ s

Small Lab (Density D_{S1})									
	Detection-AVR			Detection-VDS			Detection-LRT		
ΔT	TP	FP	Acc	TP	FP	Acc	TP	FP	Acc
1 s	0.85	0.26	0.795	0.82	0.18	0.82	0.91	0.05	0.93
3 s	0.84	0.32	0.76	0.85	0.22	0.815	0.9	0.05	0.925
5 s	0.81	0.32	0.745	0.81	0.21	0.8	0.91	0.12	0.895
Large Classroom (Density D_{L1})									
	Detection-AVR			Detection-VDS			Detection-LRT		
ΔT	TP	FP	Acc	TP	FP	Acc	TP	FP	Acc
1 s	0.82	0.27	0.78	0.84	0.19	0.8	0.92	0.1	0.91
3 s	0.79	0.31	0.74	0.85	0.215	0.79	0.9	0.11	0.895
5 s	0.77	0.35	0.715	0.79	0.23	0.775	0.88	0.2	0.85

Detection accuracy. We investigate the detection accuracy of our proposed speed change detection schemes by first using the experimental scenario in the small lab with density D_{S1} and the large classroom with density D_{L1} with time interval $\Delta T = 1, 3, 5$ s. We set scheme parameters as: $\tau_1 = 0.7$, $\tau_2 = 2.2$, and $\varepsilon = 0.6$ for small lab, and $\tau_1 = 0.64$, $\tau_2 = 1.8$, and $\varepsilon = 0.55$ for large classroom. The thresholds used in our detection schemes are empirical. We could obtain these thresholds by configuring only once for each test bed. The detection results are shown in Table 2. We observe that in both small lab and large classroom Detection-LRT scheme performs the best among these three schemes. It has the detection accuracy above 92 percent with only 5 percent false negative rate under the time interval of 1 and 3 s in the small lab. Whereas in the large classroom, the detection accuracy is around 90 percent with around 10 percent false negative rate under the time interval of 1 and 3 s. We notice that Detection-AVR performs the worst with around 75 percent accuracy. This is not surprising because Detection-AVR only utilizes averaged variance for speed change detection without leveraging fine-grained information of variance distribution. We also find that the increased detection time interval degrades the detection performance. This is because the large detection time interval flattens out the granularity of the information obtained from the RSS measurements. The larger the interval is, the more blurriness the results are. We thus choose $\Delta T = 1$ s for the rest of our study.

Impact of link density. In this study, we vary the link density from $D_{S1} \rightarrow D_{S4}$ in the small lab environment. The results are presented in Fig. 7. We find that the decreased link density degrades the detection performance due to the less link density carries less information of the variance distribution for speed change detection. Particularly, for Detection-LRT, we observe that the detection accuracy decreases from over 90 to 70 percent, and false negative increases from 10 to 15 percent when the link density decreased from $D_{S1} \rightarrow D_{S4}$.

Scalability study. We further study the scalability of the detection schemes when applying to link density D_{L1} in the large classroom setting with time interval set to 1 s. As shown in Fig. 8, we observe that the results in the large classroom setting is slightly better than that of in the small lab when the link density is the same. This shows that our methods can be applied to different scales. Further, although D_{S4} and D_{L1} are equivalent, the number of links in the large classroom is more than that in the small lab. This indicates both the density and the number of the wireless links have impact on the detection performance.

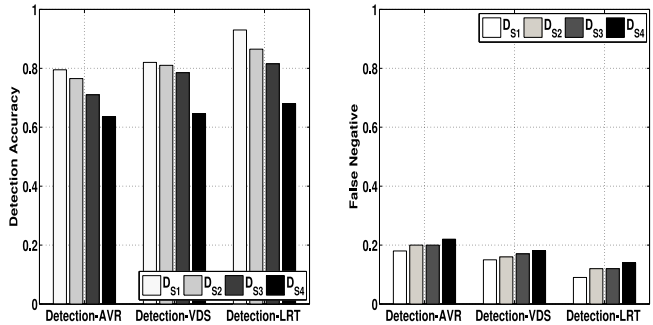

(a) Detection accuracy (b) False negative

Fig. 7. Impact of link density on detection schemes when time interval ΔT is set to 1s in the small lab.

6 Window Size Determination

In this section, we describe our window size determination scheme to adaptively update the window size for RSS variance calculation for target localization. It includes two steps: sampling check and window size determination.

Sampling check. Once the speed change is detected, we need to update the system parameter, particularly the window size for RSS variance calculation based on the changes in speed. We first use sampling check to determine whether the previous time interval for target localization encounter *Under-sampling* or *Over-sampling*, as discussed in Section 4. We compare the averaged variance over all the wireless links in current observed samples and previous observed samples. If the averaged variance in current observed samples is larger than that in the previous observed samples, we declare *Over-sampling* indicating the time-window size for variance calculation in target localization should be reduced (i.e., the target is moving faster). Otherwise, it is *Under-sampling*, which means we need to update the time-window size by increasing it (i.e., the target is moving slower).

Window size determination. We utilize a binary search based method to determine the appropriate time-window size after sampling check. We define an indicator as $I_W = \frac{1}{L}\sum_{l=1}^{L} \frac{\hat{\sigma}^2_{l,W}}{\hat{\sigma}^2_{l,W-1}}$ to adaptively determine the window size. For over-sampling scenario, we cautiously update the window size as $W \longleftarrow \frac{W}{2}$ (i.e., reduce the window size by half each time), till $0 < I_{\frac{W}{2}} - I_W < \theta$. Similarly, for under-sampling scenario, we cautiously update the window size as $W \longleftarrow 2W$ (i.e., twice the window size each time), till $-\theta < I_{2W} - I_W < 0$. After window size determination, we utilize the updated window size in localization algorithms for target localization. We note that if we can run all possible time-window sizes in parallel, we are able to derive an upper bound for the performance of our approach. We

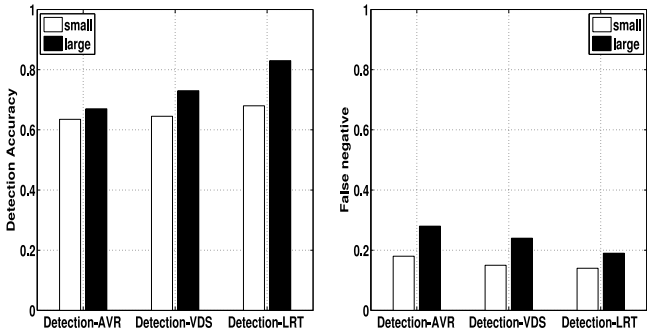

(a) Detection accuracy (b) False negative

Fig. 8. Impact of scalability on detection schemes when link density is set to D_{S4} in the small lab, and D_{L1} in the large classroom, and time interval ΔT is set to 1s.

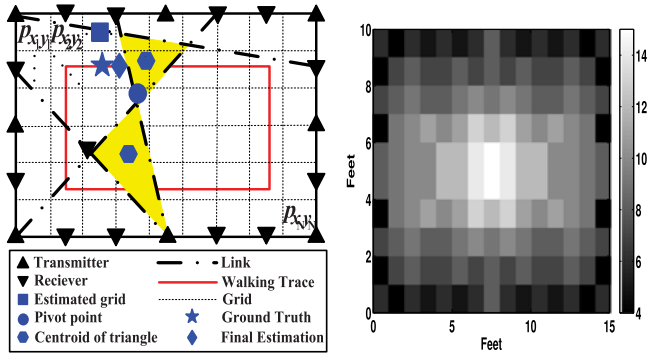

(a) (b)

Fig. 9. (a) Illustration of Localization-RIG algorithm, and (b) the number of links that pass each grid in area of interest.

would like to take this as our future work to further quantify the accuracy of our framework.

Performance evaluation. We measure the sampling check performance by computing the *accuracy of sampling check*. That is how accurate the sampling check determines *Over-sampling* and *Under-sampling*. The window size determination performance could be measured by examining the localization performance, which will be presented in Section 7. Empirically, we set the parameter $\theta = 0.3$ and 0.26 for the small lab and the large classroom respectively.

Accuracy. Table 3 shows the accuracy of sampling check under different link densities with different observed samples in both the small lab and the large classroom settings. We find that the accuracy is all over 90 percent, and as high as 98 percent when the number of observed samples are 4 and 12 under link density D_{S1} in the small lab. We also notice that the accuracy is not sensitive to the system parameters, i.e., link density and number of observed samples, although the accuracy decreases slightly when the link density decreases or the number of observed samples changes in both the small lab and the large classroom.

7 Passive Localization

In this section, we first introduce our new localization algorithm named as Reshaping-Involved Grid Reconstruction (Localization-RIG), and two existing representative algorithms (Radio Tomographic Imaging (Localization-RTI) and Intersection Method (Localization-ISM)) that we utilize to validate our proposed framework. We then evaluate the localization performance through the impact of speed change detection schemes, incorporating different localization algorithms, and the impact of link density.

TABLE 3
Accuracy of Sampling Check in Two Scales of Testbeds: Small Lab and Large Classroom with Different Densities when the Number of Observed Samples S per Transmitter and Receiver Pair are 4, 12, and 20

	Small lab				Large classroom			
S	D_{S1}	D_{S2}	D_{S3}	D_{S4}	D_{L1}	D_{L2}	D_{L3}	D_{L4}
4	0.98	0.96	0.94	0.93	0.95	0.94	0.92	0.92
12	0.98	0.95	0.95	0.93	0.94	0.93	0.92	0.91
20	0.96	0.93	0.92	0.91	0.93	0.93	0.91	0.9

7.1 Localization Algorithms

7.1.1 Reshaping-Involved Grid Reconstruction (Localization-RIG)

Our proposed algorithm is inspired by Algebraic Reconstruction in computational tomography to avoid tedious environmental parameter tuning when performing passive localization. It consists of two main steps: grid reconstruction and triangle reshaping.

Step 1: Grid reconstruction. We first divide the area of interest into multiple grids as illustrated in Fig. 9a. Each grid has multiple wireless links going through it. The basic idea is to locate the grid (x, y) that contains the largest accumulated RSS variance from all the links passing through it and return the coordinate of that grid as the initial estimation of the target's position. For a particular link l, the RSS variance $\hat{\sigma}^2_{l,W}$ can be calculated based on Equation (1) with W determined adaptively from Section 6. We then define p_{x_j,y_j} as the value of the jth grid (x_j, y_j) indicating the accumulated RSS variance from all the links passing through it. The relationship between $\hat{\sigma}^2_{l,W}$ and p_{x_j,y_j} is $\hat{\sigma}^2_{l,W} = \sum_{j=1}^{N_p} a_{l,j} p_{x_j,y_j}$, where $a_{l,j}$ is called the attenuation coefficient for the jth grid and lth link with $j = \{1 \cdots N_p\}$ and N_p is the total number of grids. The attenuation coefficient is determined by the contribution of the variance of the lth link to the jth grid. We define $a_{i,j}$ as below:

$$a_{l,j} = \begin{cases} 1, & d \le \frac{d_g}{2}, \\ 0, & otherwise, \end{cases} \tag{15}$$

where d is the distance between the center of jth grid and link l, and d_g is the half width of each square grid. We need to locate the grid with the largest value of p_{x_j,y_j} to obtain the location estimation of the target. Thus, the relationship between RSS variance vector $\hat{\boldsymbol{\sigma}}^2_{\boldsymbol{W}} = [\hat{\sigma}^2_{1,W}, \hat{\sigma}^2_{2,W}, \ldots, \hat{\sigma}^2_{L,W}]^T$ and $\mathbf{p} = [p_{x_1,y_1}, p_{x_2,y_2}, .., p_{x_{N_p},y_{N_p}}]^T$ can be described as a set of linear equations:

$$\hat{\boldsymbol{\sigma}}^2_{\boldsymbol{W}} = \mathbf{A}\mathbf{p}, \tag{16}$$

where $\mathbf{A}$ is a $L \times N_p$ matrix with each column describing a single grid and each row representing the attenuation

coefficient of the ith grid for the lth link. Based on algebraic reconstruction [40], Equation (16) can be solved by reconstructing the value of each grid:

$$p_{x_j,y_j} = \frac{1}{L_{p_j}} \sum_{l=1}^{L_p} \frac{\hat{\sigma}_{l,W}^2}{d_l}, \tag{17}$$

where $L_{p_j} = \sum_{l=1}^{L} a_{l,j}$ is the number of links that cross the jth grid and d_l is the distance between transmitter and receiver in lth link. Step 1 obtains $p_{x,y} = \max\{p_{x_j,y_j}\}$ and returns (x, y) as the initial position estimation of the target.

The Grid Reconstruction provides the useful information of the initial position estimation of the target, however, we find that the position estimate (marked as square) is biased and located farther away from the center of the area as comparing to the true target location (marked as star) as shown in Fig. 9a. This is because Grid Reconstruction takes into account of all the links going through a grid. And it is intuitive that geometrically the number of links in the area closer to the center is more than those in the area away from the center. We illustrate this phenomenon in Fig. 9b. Thus, during the calculation of the accumulated RSS variance, the grids closer to the center will result in relative smaller RSS variance values due to the large number of wireless links may contain RSS variance value falling beyond the range of $3\sigma_{l,W}$, making the initial position estimation biased to be farther away from the center.

Step 2: Triangle reshaping. The objective of Step 2 is to reduce the location estimation bias introduced in Step 1 by exploiting only those links with large RSS variance values in each grid. In particular, we seek to find a pivot point by forming virtual triangles consisting of links with large RSS variance values. For each grid, we consider L_K (with $L_K \leq L$) links with top L_K RSS variance values. We choose any three links out of L_K to form a virtual triangle. There will be maximum L_{max} (with $L_{max} \leq \binom{L_K}{3}$) number of triangles and each triangle yields a centroid location. We define the pivot point (x_{pivot}, y_{pivot}) as the weighted average of all the triangle centroids:

$$x_{pivot} = \frac{\sum_{j=1}^{L_{max}} \omega_j x_j}{\sum_{j=1}^{L_{max}} \omega_j}, y_{pivot} = \frac{\sum_{j=1}^{L_{max}} \omega_j y_j}{\sum_{j=1}^{L_{max}} \omega_j}, \tag{18}$$

where (x_j, y_j) is the centroid of the jth virtual triangle; ω_j is the weight of the triangle and equals to the sum of RSS variance of three links forming the triangle. Fig. 9a depicts the scenario of obtaining the pivot point (represented as circle) by weighted average of the centroid of two triangles (marked as triangle). We notice that the resulting pivot point tends to be closer to the center comparing to the true location of the target. Thus, by leveraging this pivot point, the target position estimation (marked as diamond) could be obtained as the middle point of the initial estimation from Grid Reconstruction and the pivot point.

7.1.2 Existing Methods

Besides our proposed Localization-RIG method, we also evaluate the performance of two representative passive localization algorithms under our framework.

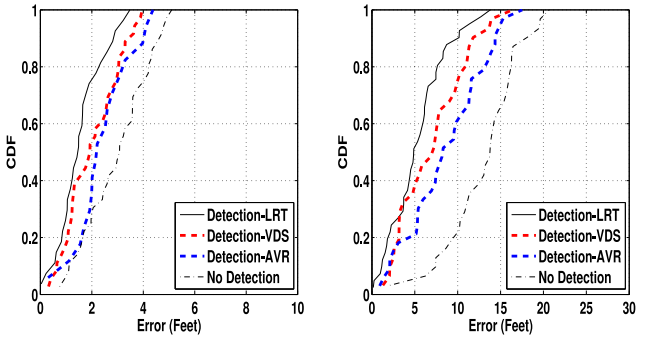

(a) small lab with density D_{S1} (b) large classroom with density D_{L1}

Fig. 10. Impact of speed change detection schemes on passive localization: CDF of localization error comparison when using Localization-RIG under three speed change detection schemes and without speed change detection.

Radio tomographic imaging (Localization-RTI). This method takes advantage of the variance of RSS measurements caused by the moving target in the wireless environment. The signal strength of a wireless link is dependent on the power that travels through space containing moving targets. A linear model relating variance of RSS measurements to physical locations of moving target is introduced and utilized to obtain estimation of a motion image. Tikhonov regularization is utilized to solve the set of linear equations formulated by either the variance or the mean of RSS measurements. Valuable noise models are derived based on real measurements of a deployed RTI system [8], [11].

Intersection method (Localization-ISM). This method constructs a signal dynamic model to obtain the changing behaviors of RSS variance caused by the moving targets. It utilizes the RSS variance between the static environment and the dynamic environment to estimate the location of target. The coordinates are derived from the intersection of any two influential links. The weight of the two intersected influential links is defined as the sum of the RSS change of the two influential links. The final estimation is calculated as the weighted average value of all the intersection points [7].

7.2 Performance Evaluation

7.2.1 Impact of Speed Change Detection Schemes

We first analyze the impact of speed change detection schemes on passive localization performance. We show the cumulative distribution function (CDF) of the localization error, the distance between the estimated location to the true target location, when using proposed Localization-RIG method under three speed change detection schemes with time interval set to 1 s as shown in Fig. 10 in both the small lab as well as the large classroom environments. We observe that localization performance has been improved largely when the speed change detection schemes are applied. Specifically, in the small lab, the median error decreases from 3 ft under no speed change detection to around 1.8 ft under Detection-LRT (40 percent improvement), and the maximum error decreases from 5 to 3.5 ft (30 percent improvement). While in the large classroom, the median error decreases from 12 ft under no speed change detection to 5 ft under Detection-LRT (over 50 percent improvement), and the maximum error decreases from 20 to 14 ft (30 percent improvement).

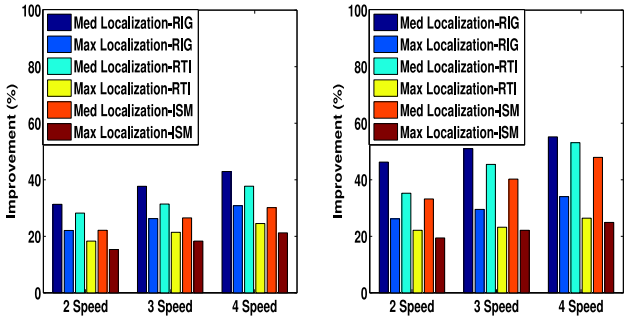

(a) small lab with density D_{S1} (b) large class room with density D_{L1}

Fig. 11. Percentage of localization improvement of three localization algorithms when using our framework (Detection-LRT) over that without using our framework considering different target speeds.

Furthermore, examining the localization performance among three speed change detection schemes, Detection-LRT produces the best localization performance on both median and maximum errors as compared to the localization conducted under the other two speed change detection schemes (Detection-VDS and Dection-AVR). In particular, in the large classroom, comparing to Detection-VDS and Detection-AVR, the median error of Detection-LRT decreases from around 7.5 to 5 ft (33 percent improvement), and the maximum error deceases from around 18 to 14 ft (22 percent improvement). This is because Detection-LRT has the best speed change detection accuracy among the speed change detection schemes. This is inline with our previous results as shown in Figs. 7 and 8. These observations are very encouraging as it indicates that our speed change detection framework is highly effective to produce accurate passive localization results when target travels with dynamic speeds.

7.2.2 Incorporating Different Localization Algorithms

We next study the performance of our framework by comparing the performance of different passive localization algorithms when they use our framework. There is no additional setup cost for these localization schemes. Fig. 11 depicts the bar graph of the percentage of localization improvement when using our framework (i.e., using Detection-LRT) to that without using our framework (i.e., no speed change detection). This study involves two, three and four different target speeds for both experimental setups in the small lab and the large classroom. In general, for all of three passive localization algorithms, the localization performance improves when using our framework with speed change detection. We observe that there are $30-40$ percent improvement on median error and $20-30$ percent improvement on maximum error when using our framework versus no framework applied in the small lab. While in the large classroom, the improvement increases to 50 percent on median error and 30 percent on maximum error.

We then compare the performance of our proposed Localization-RIG over the other two existing localization algorithms. We find that Localization-RIG outperforms the other two existing algorithms up to 15 percent on median error and 20 percent when on maximum error in both the small lab and the large classroom. When comparing to Localization-ISM, the localization improvement of our proposed Localization-RIG increases 20 percent on median error and 15 percent on maximum error. By comparing Localization-RTI to Localization-RIG, there are around 15 percent improvement on median error, and 10 percent improvement on maximum error by using our proposed Localization-RIG. This is because in our proposed localization algorithm, we utilize Triangle Reshaping step by exploiting those links with large RSS variance values in each grid to reduce the location estimation bias, which is introduced by the Grid Reconstruction step.

TABLE 4
Average Time Cost per Location Estimation of Localization Algorithms in the Small Lab with Link Density D_{S1}

	Localization-RIG	Localization-RTI	Localization-ISM
Time cost (s)	0.028	0.016	0.011

Furthermore, we examine the localization improvement using our framework by increasing the number of involved speed change over that without using our framework. We observe that the localization improvement increases as the number of involved speed change increases. In particular, we find that the localization improvement of Localization-RIG exhibits from 30 percent to over 40 percent on median error and from 20 to 30 percent on maximum error when the number of involved speeds increases from 2 to 4 in the small lab. We observe the similar trend in the large classroom as well. These observations suggest that our framework is not only generic across different algorithms, but also becomes more effective when the mobility dynamics increases.

Time cost. We further study the time performance of the localization algorithms by measuring the average time cost per location estimation. Table 4 presents the average time cost per location estimation over 600 testing points in the small lab with link density D_{S1}. We find that Localization-RIG takes longer time than other two localization algorithms because it includes more steps (Grid Reconstruction and Triangle Reshaping) in location estimation. We note that there is a trade off between the accuracy and time cost in choosing the localization algorithms. But, overall the time cost is modest and remains in millisecond level.

7.2.3 Impact of Link Density

We study the impact of link density on the localization performance when density varies from D_{S1} to D_{S4} in the small lab and from D_{L1} to D_{L4} for the large classroom. Fig. 12 presents the boxplot of localization error when using Localization-RIG with Detection-LRT scheme. We observe that higher link density improves localization accuracy and makes localization performance more stable for the small lab as well as in the large classroom. Specifically, the median error decreases from 5 to around 1.2 ft when the link density increases from D_{S4} to D_{S1} in the small lab. While in the large classroom, the median error decreases from 17 to around 5.5 ft when the link density increases from D_{L4} to D_{L1}. The variation of the localization error is significantly reduced especially in the small lab when the link density increases from D_{S4} to D_{S1}. We note that the link density of D_{S4} is

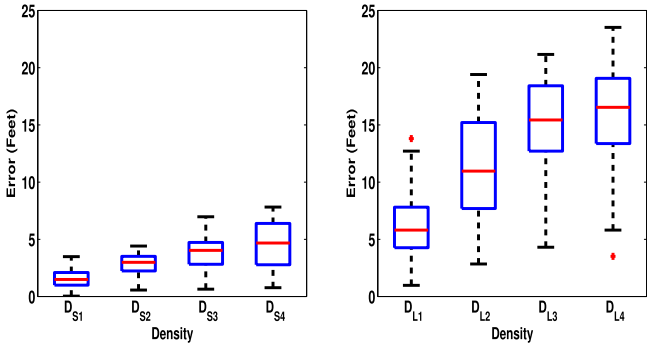

(a) small lab (b) large classroom

Fig. 12. Impact of link density: boxplot of localization performance when applying Localization-RIG under Detection-LRT.

equivalent to D_{L1}, which yields comparable median errors in both the small lab and the large classroom. However, larger maximum error incurred in the large classroom scenario is due to rich multi-path effects and much more sparse link density in the large classroom.

8 Concluding Remarks

In this paper, we investigate how to improve the performances of device-free passive localization when targets are traveling at dynamic speeds. Along this line, we propose an adaptive speed change detection framework with three main components: speed change detection, adaptive time-window size selection, and passive localization. Three speed change detection schemes are also designed based on statistical learning from the information obtained by RSS measurements. Furthermore, we develop a new device-free localization algorithm, named RIG, which is inspired by Algebraic Reconstruction in computational tomography. RIG does not require tedious environmental parameter tuning when performing passive localization. Finally, extensive experiments in a real-world environment are provided to show the effectiveness of our proposed framework. The results show significant improvement on localization performance (50 percent improvement on median error and 30 percent improvement on maximum error) compared to existing device-free localization systems without using our framework.

Acknowledgments

The authors would like to thank Yu Gan for helping conduct experiments and performing localization activities in this project. The preliminary results have been published in "Adaptive Device-Free Passive Localization Coping with Dynamic Target Speed" [41] in IEEE International Conference on Computer Communications (INFOCOM), Mini Conference, 2013. This project was supported in part by US National Science Foundation (NSF) Grants CCF1018270, CNS1217387, CNS1016303, CNS1409652, CNS1409767, CCF1018151 and IIS1256016.

References

[1] M. Youssef, M. Mah, and A. Agrawala, "Challenges: Device-free passive localization for wireless environments," in *Proc. ACM Int. Conf. Mobile Comput. Netw.* 2007, pp. 222–229.

[2] J. Yang, Y. Ge, H. Xiong, Y. Chen, and H. Liu, "Performing joint learning for passive intrusion detection in pervasive wireless environments," in *Proc. IEEE Int. Conf. Comput. Commun.*, Mar. 2010, pp. 1–9.

[3] C. Xu, B. Firner, Y. Zhang, R. Howard, J. Li, and X. Lin, "Improving RF-based device-free passive localization in cluttered indoor environments through probabilistic classification methods," in *Proc. Int. Conf. Inform. Process. Sens. Netw.*, 2012, pp. 209–220.

[4] P. Bahl and V. N. Padmanabhan, "RADAR: An in-building RF-based user location and tracking system," in *Proc. IEEE Int. Conf. Comput. Commun.*, Mar. 2000, pp. 775–784.

[5] J. Yang and Y. Chen, "Indoor localization using improved RSS-based lateration methods," in *Proc. IEEE Global Commun. Conf.*, Nov. 2009, pp. 1–6.

[6] H. Liu, Y. Gan, J. Yang, S. Sidhom, Y. Wang, Y. Chen, and F. Ye, "Push the limit of WiFi based localization for smartphones," in *Proc. Int. Conf. Mobile Comput. Netw.*, Aug. 2012, pp. 305–316.

[7] D. Zhang, J. Ma, Q. Chen, and L. M. Ni, "An RF-Based System for Tracking Transceiver-Free Objects," in *Proc. IEEE Int. Conf. Pervasive Comput. Commun.*, Mar. 2007, pp. 135–144.

[8] J. Wilson and N. Patwari, "See-Through Walls: Motion Tracking Using Variance-Based Radio Tomography Networks," *IEEE Trans. Mobile Comput.*, vol. 10, no. 5, pp. 612–621, May 2011.

[9] C. Chang and A. Sahai, "Object tracking in a 2D UWB sensor network," in *Proc. 38th Asilomar Conf. Signals, Syst. Comput.*," Nov. 2004, vol. 1, pp. 1252–1256.

[10] T. Pratt, S. Nguyen, and B. T. Walkenhorst, "Dual-polarized architectures for sensing with wireless communications signals," in *Proc. IEEE Military Commun. Conf.*, Nov. 2008, pp. 1–6.

[11] J. Wilson and N. Patwari, "Radio tomographic imaging with wireless networks," *IEEE Trans. Mobile Comput.*, vol. 9, no. 5, pp. 621–632, May 2010.

[12] D. Zhang, Y. Yang, D. Cheng, S. Liu, and L. M. Ni, "COCKTAIL: An RF-based hybrid approach for indoor localization," in *Proc. IEEE Int. Conf. Commun.*, May 2010, pp. 1–5.

[13] G. T. Herman, *Fundamentals of Computerized Tomography: Image reconstruction from projections*. New York, NY, USA: Springer, 2009.

[14] Y. Yang and A. E. Fathy, "See-through-wall imaging using ultra-sideband short-pulse radar system," in *Proc. IEEE Antennas Propagation Soc. Int. Symp.*, Jul. 2005, pp. 334–337.

[15] F. Viani, L. Lizzi, P. Rocca, M. Benedetti, M. Donelli, and A. Massa, "Object tracking through RSSI measurements in wireless sensor networks," *Electron. Lett.*, vol. 44, pp. 653–654, May 2008.

[16] F. Viani, P. Rocca, M. Benedetti, G. Oliveri, and A. Massa, "Electromagnetic passive localization and tracking of moving targets in a WSN-infrastructured environment," *Inverse Problem*, vol. 26, Mar. 2010.

[17] D. Zhang and L. M. Ni, "Dynamic clustering for tracking multiple transceiver-free objects," in *Proc. IEEE Int. Conf. Pervasive Comput. Commun. Conf.*, Mar. 2009, pp. 1–8.

[18] M. Moussa and M. Youssef, "Smart devices for smart environments: Device-free passive detection in real environments," in *Proc. IEEE Int. Conf. Pervasive Comput. Commun.*, Mar. 2009, pp. 1–6.

[19] M. Seifeldin and M. Youssef, "A deterministic large-scale device-free passive localization system for wireless environments," in *Proc. Int. Conf. Pervasive Technol. Related Assist. Environ.*, 2010, pp. 51:1–51:8.

[20] M. Seifeldin, A. Saeed, A. Kosba, A. El-keyi, and M. Youssef, "Nuzzer: A large-scale device-free passive localization system for wireless environments," *IEEE Trans. Mobile Comput.*, vol. 12, no. 7, pp. 1321–1334, Jul. 2013.

[21] F. Viani, M. Martinelli, L. Ioriatti, M. Benedetti, and A. Massa, "Passive real-time localization through wireless sensor networks," in *Proc. IEEE Int. Symp. Geosci. Remote Sens.*, Jul. 2009, vol. 2, pp. 718–721.

[22] F. Viani, M. Donelli, M. Salucci, P. Rocca, and A. Massa, "Opportunistic exploitation of wireless infrastructures for homeland security," in *Proc. IEEE AP-S Int. Symp.*, Jul. 2011, pp. 3062–3065.

[23] F. Viani, P. Rocca, G. Oliveri, D. Trinchero, and A. Massa, "Localization, tracking, and imaging of targets in wireless sensor networks," *Radio Sci.*, vol. 46, Oct. 2011.

[24] F. Viani, F. Robol, A. Polo, P. Rocca, G. Oliveri, and A. Massa, "Wireless architectures for heterogeneous sensing in smart home applications-concepts and real implementations," *Proc. IEEE*, vol. 101, no. 11, pp. 2381–2396, Nov. 2013.

[25] M. A. Kanso and M. G. Rabbat, "Compressed RF tomography for wireless sensor networks: Centralized and decentralized approaches," in *Proc. IEEE Int. Conf. Distrib. Comput. Sens. Syst.*, 2009, pp. 173–186.
[26] Y. Zhao and N. Patwari, "Noise reduction for variance-based device-free localization and tracking," in *Proc. IEEE Commun. Soc. Conf. Sens., Mesh Ad Hoc Commun. Netw.*, 2011, vol. 10, pp. 612–621.
[27] X. Chen, A. Edelstein, Y. Li, M. Coates, M. G. Rabbat, and A. Men, "Sequential Monte Carlo for simultaneous passive device-free tracking and sensor localization using received signal strength measurements," in *Proc. ACM/IEEE Conf. Inform. Process. Sens. Netw.*, Apr. 2011, pp. 342–353.
[28] Y. Li, X. Chen, M. Coates, and B. Yang, "Sequential Monte Carlo Radio-Frequency Tomographic Tracking," in *Proc. Int. Conf. Acoustics, Speech, Signal Process.*, May 2011, pp. 3976–3979.
[29] J. Wilson and N. Patwari, "A fade level skew-laplace signal strength model for device-free localization with wireless networks," *IEEE Trans. Mobile Comput.*, vol. 11, no. 6, pp. 947–958, Jun. 2012.
[30] A. E. Kosba, A. Saeed, and M. Youssef, "RASID: A robust WLAN device-free passive motion detection system," in *Proc. IEEE Int. Conf. Pervasive Comput. Commun.*, Mar. 2012, 180–189.
[31] A. Saeed, A. E. Kosba, and M. Youssef, "Ichnaea: A low-overhead robust WLAN device-free passive localization system," *IEEE J. Sel. Topics Signal Process.*, vol. 8, no. 1, pp. 5–15, Feb. 2014.
[32] B. Firner, S. Medhekar, Y. Zhang, R. Howard, and W. Trappe, "PIP Tags: Hardware design and power optimization," in *Proc. 5th Workshop Embedded Netw. Sens.*, Mar. 2008.
[33] B. Firner, P. Jadhav, Y. Zhang, R. Howard, W. Trappe, and E. Fenson, "Towards continuous asset tracking: Low-power communication and fail-safe presence assurance," in *Proc. IEEE Commun. Soc. Conf. Sens., Mesh Ad Hoc Commun. Netw.*, Jun. 2009, pp. 1–9.
[34] R. C. Browning, E. A. Baker, J. A. Herron, and R. Kram, "Effects of obesity and sex on the energetic cost and preferred speed of walking," *Appl. Physiol.*, vol. 100, pp. 390–398, 2005.
[35] N. Kassem, A. E. Kosba, and M. Youssef, "RF-based vehicle detection and speed estimation system," in *Proc. IEEE Veh. Technol. Conf.*, May 2012, pp. 1–5.
[36] A. Al-Husseiny and M. Youssef, "RF-based Traffic Detection and Identification," in *Proc. IEEE Vehicular Technol. Conf.*, Sep. 2012, pp. 1–5.
[37] H. Zhu, "On information and sufficiency," *Ann. Math. Stat.*, vol. 22, pp. 79–86, 1951.
[38] P. G. Moschopoulos and W. B. Canada, "The distribution function of a linear combination of chi-squares," *Comput. Math. Appl.*, vol. 10, pp. 383–386, 1984.
[39] J. Aldrich and R. A. Fisher, "The making of maximum likelihood 1912-1922," *Statist. Sci.*, vol. 12, pp. 162–176, 1997.
[40] D. Raparia, J. Alessi, and A. Kponou, "The Algebraic Reconstruction Technique (ART)," in *Proc. Particle Accelerator Conf.*, May 1997, pp. 2023–2025.
[41] X. Zheng, J. Yang, Y. Chen, and Y. Gan, "Adaptive device-free passive localization coping with dynamic target speed," in *Proc. IEEE Int. Conf. Comput. Commun. Mini Conf.*, Apr. 2013, pp. 485–489.

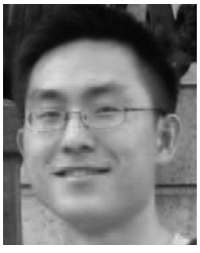

Xiuyuan Zheng received the bachelor's degree from the Department of Telecommunication Engineering, Nanjing University of Posts and Communications, China, in 2007. He is currently working toward the PhD degree in the Department of Electrical and Computer Engineering Stevens Institute of Technology. His current research interests include information security and privacy, wireless localization and location based services (LBS), wireless and sensor networks. He is currently with the Data Analysis and Information SecuritY (DAISY) Lab with Prof. Yingying Chen. He was in the Master program in the Department of Electrical and Computer Engineering, Stevens Institute of Technology from 2007 to 2009.

Jie Yang received the PhD degree in computer engineering from Stevens Institute of Technology in 2011. He is currently an assistant professor in the Department of Computer Science at Florida State University. His current research interests include cyber security and privacy, and mobile and pervasive computing, with an emphasis on network security, smartphone security and applications, security in cognitive radio and smart grid, location systems and vehicular applications. His research is supported by National Science Foundation (NSF) and Army Research Office (ARO). He received the Best Paper Runner-up Award from IEEE Conference on Communications and Network Security (CNS) in 2013 and the Best Paper Award from ACM MobiCom in 2011. His research has received wide press coverage including *MIT Technology Review*, *The Wall Street Journal*, NPR, CNET News, and Yahoo News. He is a member of the IEEE.

Yingying (Jennifer) Chen received the PhD degree in computer science from Rutgers University. She is currently an associate professor in the Department of Electrical and Computer Engineering at Stevens Institute of Technology. Her current research interests include cyber security and privacy, mobile computing, mobile healthcare, and wireless networks. She has published extensively in these areas in both journal articles and referred conference papers. Prior to joining Stevens University , she was with Alcatel-Lucent. She received the US National Science Foundation (NSF) CAREER Award and Google Research Award. She also received the NJ Inventors Hall of Fame Innovator Award. She received the Best Paper Award from ACM International Conference on Mobile Computing and Networking (MobiCom) in 2011. She also received the IEEE Outstanding Contribution Award from IEEE New Jersey Coast Section each year from 2005 to 2009. Her research has been reported in numerous media outlets.

Hui Xiong received the BE degree from the University of Science and Technology of China, China, the MS degree from the National University of Singapore, Singapore, and the PhD degree from the University of Minnesota. He is currently an associate professor and the vice chair at the Department of Management Science and Information Systems, and the director of Rutgers Center for Information Assurance at the Rutgers, the State University of New Jersey, where he received a two-year early promotion/tenure in 2009, the Rutgers University Board of Trustees Research Fellowship for Scholarly Excellence in 2009. His current research interest includes data and knowledge engineering, with a focus on developing effective and efficient data analysis techniques for emerging data intensive applications. He has published prolifically in refereed journals and conference proceedings (three books, 40+ journal papers, and 60+ conference papers). He is a co-editor-in-chief of the *Encyclopedia of GIS*, an associate editor of the *IEEE Transactions on Data and Knowledge Engineering* and the *Knowledge and Information Systems* journal. He has served regularly on the organization and program committees of numerous conferences, including as a Program Co-Chair of the Industrial and Government Track for the 18th ACM SIGKDD International Conference on Knowledge Discovery and Data Mining and a Program co-chair for the 2013 IEEE International Conference on Data Mining. He is a senior member of the ACM and the IEEE. He received the Best Research Paper Award from the IEEE International Conference on Data Mining in 2011.